

Optimized probes of CP -odd effects in the $t\bar{t}h$ process at hadron colliders

Blaž Bortolato^a, Jernej F. Kamenik^{a,b}, Nejc Košnik^{a,b}, Aleks Smolkovič^a

^a*J. Stefan Institute, Jamova 39, P. O. Box 3000, 1001, Ljubljana, Slovenia*

^b*Department of Physics, University of Ljubljana, Jadranska 19, 1000 Ljubljana, Slovenia*

Abstract

We use machine learning (ML) and non-ML techniques to study optimized CP -odd observables, directly and maximally sensitive to the CP -odd $i\tilde{\kappa}\bar{t}\gamma^5t h$ interaction at the LHC and prospective future hadron colliders using the final state with a Higgs boson and a top quark pair, $pp \rightarrow t\bar{t}h$, followed by semileptonic t decays. We perform phase-space optimization of manifestly CP -odd observables (ω), sensitive to the sign of $\tilde{\kappa}$, and constructed from experimentally accessible final state momenta. We identify a simple optimized linear combination $\alpha \cdot \omega$ that gives similar sensitivity as the studied fully fledged ML models. Using $\alpha \cdot \omega$ we project the expected sensitivities to $\tilde{\kappa}$ at HL-LHC, HE-LHC, and FCC-hh.

Keywords: top quark physics, CP violation, beyond the Standard Model, machine learning

1. Introduction

The interaction between the heaviest particles of the Standard Model (SM), the top quark t and the Higgs boson h , is well known in the SM. The measured top quark mass m_t and the electroweak condensate value v precisely determine the on-shell scalar coupling $-y_t\bar{t}th$ to be $y_t = \sqrt{2}m_t/v$, while the P - and CP -odd interaction $\bar{t}\gamma^5t h$ is absent. Beyond the SM, effective operators of dimension-6 can break this correlation and result in more general (pseudo)scalar $\bar{t}th$ couplings κ ($\tilde{\kappa}$) [1],

$$\mathcal{L}_{ht} = -\frac{y_t}{\sqrt{2}}\bar{t}(\kappa + i\tilde{\kappa}\gamma_5)th, \quad (1)$$

which reduce to the SM case at $\kappa = 1$, $\tilde{\kappa} = 0$. At the LHC it is possible to probe these couplings directly with two of the particles in Eq. (1) on-shell¹ in top-Higgs associated production processes $pp \rightarrow thj$ and $pp \rightarrow t\bar{t}h$ [2–22]². The corresponding total cross sections scale as κ^2 , $\tilde{\kappa}^2$ (thj also as κ), and are thus poorly sensitive to small nonzero $\tilde{\kappa}$. Linear sensitivity to $\tilde{\kappa}$ on the other hand can be achieved by measuring P - and CP -odd observables.

¹Since $m_h < 2m_t$ one cannot probe these couplings with all the three particles on-shell.

²The loop induced partonic process $gg \rightarrow h \rightarrow t\bar{t}$ depends on κ^2 , κ , and $\tilde{\kappa}^2$ already on the production side as it is dominated by the top quark loop [23].

In a recent paper we have proposed experimentally feasible and manifestly CP -odd probes of $\tilde{\kappa}$ in thj and $t\bar{t}h$ final states at the LHC and prospective future hadron colliders [24]. The overwhelming irreducible backgrounds make the thj channel impractical. For the $t\bar{t}h$ case we have identified 13 different CP -odd observables that can be constructed out of 5 measurable final state momenta and an additional triple-product asymmetry [25]. Namely, assuming $pp \rightarrow t\bar{t}h$ production with semileptonically decaying tops, we combined the final state lepton momenta $\mathbf{p}_{\ell^+}, \mathbf{p}_{\ell^-}$, two b -jet momenta $\mathbf{p}_b, \mathbf{p}_{\bar{b}}$ (although without discriminating their charges³) and the Higgs momentum \mathbf{p}_h in different ways to construct C -even, P -odd laboratory frame observables ω_i [24]. Note that the Higgs momentum \mathbf{p}_h can be reconstructed in any feasible final state in the approach we propose. We have singled out the observable with the largest individual sensitivity to $\tilde{\kappa}$, namely

$$\omega_6 \sim [(\mathbf{p}_{\ell^-} \times \mathbf{p}_{\ell^+}) \cdot (\mathbf{p}_b + \mathbf{p}_{\bar{b}})] [(\mathbf{p}_{\ell^-} - \mathbf{p}_{\ell^+}) \cdot (\mathbf{p}_b + \mathbf{p}_{\bar{b}})]. \quad (2)$$

In Appendix A we derive the set of CP -odd observables in a systematic way, completing the set introduced in Ref. [24], so that it now contains 22 ω 's. Importantly, one among the new observables

$$\omega_{14} \sim [(\mathbf{p}_{\ell^-} \times \mathbf{p}_{\ell^+}) \cdot (\mathbf{p}_b - \mathbf{p}_{\bar{b}})] [(\mathbf{p}_b - \mathbf{p}_{\bar{b}}) \cdot (\mathbf{p}_{\ell^-} - \mathbf{p}_{\ell^+})]. \quad (3)$$

gives similar performance to ω_6 .

Due to the high dimensionality and complexity of the phase-space in this process with top quarks decaying semileptonically, in Ref. [24] we have not ventured further in the search for an optimal CP probe of the $t\bar{t}h$ interaction. The aim of the present paper is to finally tackle this problem and use the complete kinematical information accessible experimentally to construct an optimal CP -odd observable. To this end we rely on neural networks (NN) trained on Monte-Carlo generated samples to efficiently parametrize the weight function of events across the multi-dimensional phase-space in order to maximize the statistical sensitivity to $\tilde{\kappa}$. We show how the required P - and CP -symmetry properties of the NN-based observables can be imposed *a priori*. Finally, we compare in terms of optimality, a general CP -odd NN function of the phase-space to a linear combination of manifestly CP -odd variables. We note that existing general purpose ML inference tools are already able to optimize sensitivity to a given parameter (see e.g. Ref. [27]). The purpose of this work is to do so in a an economic way that manifestly respects the symmetries of the problem.

The outline of this paper is as follows. In Sec. 2 we perform the phase-space optimization of ω_6 , analogous to the study of th production in Ref. [24], but now applied to a multi-dimensional phase-space of semileptonic $t\bar{t}h$ parametrized through a NN. Next, as a generalization to other available ω 's we consider a manifestly CP -odd (C -even and P -odd) observable completely parameterized by a NN. We also consider a first order approximation of this observable. In this limit, the significance optimization can be performed without the need for advanced machine learning techniques. At the same time we show that it is just slightly suboptimal compared to the fully fledged NN. We use this optimized observable in Sec. 3 to produce limits in the $\kappa - \tilde{\kappa}$ plane at HL-LHC [28–30], HE-LHC [31, 32], and FCC-hh [33–35]. We conclude in Sec. 4.

³Efficient b -jet charge discrimination could allow to construct further CP -odd observables, see e.g. [7, 26].

2. Neural network approach to the optimal CP -odd observable in $t\bar{t}h$

We implement the training and evaluation of neural networks using the `TensorFlow` framework [36]. In all cases we train on a sample of 10^7 $pp \rightarrow ht(\rightarrow b\ell^+\nu)\bar{t}(\rightarrow \bar{b}\ell^-\nu)$ events generated using `Madgraph5` [37] with $\tilde{\kappa} = 1$, and split into separate training (7.5M) and test (2.5M) samples. In the following we always set $\kappa = 1$ and only vary $\tilde{\kappa}$, without loss of generality, since the leading CP -odd differential rate is proportional to $\tilde{\kappa}\kappa$. Unless stated otherwise the results are shown for events in pp collisions at 14 TeV. We randomly initialize the neural network weights using the default Glorot uniform initializer and use the Adam optimizer with a custom varying learning rate $l(e) = l(e-1)/(1+0.8^e)$ where e is the current epoch and the initial learning rate is set to 0.1. We use `relu` for the activation function. We train all networks using the loss function

$$\text{loss}(\boldsymbol{\alpha}) = \left(\frac{\text{mean}(\mathcal{F}(\mathbf{X}; \boldsymbol{\alpha}))}{\text{std}(\mathcal{F}(\mathbf{X}; \boldsymbol{\alpha}))/\sqrt{N}} \right)^{-2}, \quad (4)$$

where the `mean()` and the standard deviation `std()` are to be calculated over all events in the sample. The loss corresponds to the inverse of the significance-squared of the observable $\mathcal{F}(\mathbf{X}; \boldsymbol{\alpha})$ that should be minimized in order to achieve optimal statistical sensitivity. Here N is the size of the sample, $\boldsymbol{\alpha}$ are the free neural network weights and biases and \mathbf{X} stands for the values of CP -even and/or CP -odd phase-space variables in the given event. We avoid over-fitting of the training sample by stopping the training when at least 30 epochs have passed and one of the following two criteria is satisfied: either the running average of 20 training losses saturates to 0.5% or the running average of 20 test losses increases for 5 epochs in a row. We keep a model history and in the end choose the best model in terms of test loss. In practice we find that mostly the first condition terminates the training loop, and the best model is usually the model from the final epoch of training. In order to determine the optimal NN architecture we perform a scan over a set of possible NN configurations with up to 2 hidden layers and up to 9 nodes per NN layer.⁴ We choose this cutoff for representational purposes, however we have checked that our results do not change significantly when using larger networks, namely up to three hidden layers of 30 nodes each.

2.1. Phase-space optimization of ω_6

Here we study the optimization of the ω_6 variable (2) based on phase-space averaging. We denote the CP -even phase-space variables with \mathbf{x} and a single CP -odd one with ω_6 . Using this notation we can write the $t\bar{t}h$ production differential cross section with semileptonically decaying tops as

$$\frac{d\sigma}{d\mathbf{x}d\omega_6} = A(\mathbf{x}, |\omega_6|) + \tilde{\kappa}\kappa B(\mathbf{x}, \omega_6). \quad (5)$$

where A is manifestly CP -even and B a CP -odd function of ω that stems from the interference of scalar and pseudoscalar amplitudes. We do not follow the optimization

⁴ We have also considered an automated algorithm to determine the optimal NN architecture (i.e. Hyperopt [38], see also Ref. [39] for one of its recent uses.). Here instead we present results of manual scans over a set of possible NN configurations in order to have better control over the NN parameters. We found the results of both approaches comparable.

procedure based on separating A and B since this would require cumbersome multidimensional binning [40]. We use a vector of easily accessible CP -even Mandelstam variables \mathbf{x} :

$$\mathbf{x} = \begin{pmatrix} (\mathbf{p}_{\ell^+} + \mathbf{p}_{\ell^-}) \cdot \mathbf{p}_h \\ (\mathbf{p}_{\ell^+} + \mathbf{p}_{\ell^-}) \cdot (\mathbf{p}_b + \mathbf{p}_{\bar{b}}) \\ (\mathbf{p}_b + \mathbf{p}_{\bar{b}}) \cdot \mathbf{p}_h \\ \mathbf{p}_{\ell^+} \cdot \mathbf{p}_{\ell^-} \\ \mathbf{p}_b \cdot \mathbf{p}_{\bar{b}} \end{pmatrix}. \quad (6)$$

Our goal is to find the optimal CP -even weight function $f(\mathbf{x}; \boldsymbol{\alpha})$, which should be used to calculate the weighted average of ω_6 . The function f takes CP -even quantities \mathbf{x} as inputs, therefore we expect its dependence on $\tilde{\kappa}$ to be of the form

$$f(\mathbf{x}; \boldsymbol{\alpha}) = C(\mathbf{x}; \boldsymbol{\alpha}) + \tilde{\kappa}^2 D(\mathbf{x}; \boldsymbol{\alpha}) + \mathcal{O}(\tilde{\kappa}^4). \quad (7)$$

Using (5) we can now express the observable as

$$\begin{aligned} \langle f(\mathbf{x}; \boldsymbol{\alpha}) \omega_6 \rangle &= \int \frac{d\sigma}{d\mathbf{x} d\omega_6} f(\mathbf{x}; \boldsymbol{\alpha}) \omega_6 d\mathbf{x} d\omega_6 \\ &= \tilde{\kappa} \kappa \int B(\mathbf{x}, \omega_6) C(\mathbf{x}; \boldsymbol{\alpha}) \omega d\mathbf{x} d\omega_6 + \tilde{\kappa}^3 \int B(\mathbf{x}, \omega_6) D(\mathbf{x}; \boldsymbol{\alpha}) d\mathbf{x} d\omega_6 + \mathcal{O}(\tilde{\kappa}^5), \end{aligned} \quad (8)$$

where the definition of the average is $\langle \# \rangle \equiv \int \frac{d\sigma}{d\mathbf{x} d\omega} \# d\mathbf{x} d\omega$. The presence of odd powers of $\tilde{\kappa}$ reflects the CP -oddness of the observable. The large dimensionality of the phase-space suggests the parameterisation of the function $f(\mathbf{x}; \boldsymbol{\alpha})$ by means of an appropriate NN. In terms of the loss function (4) we have $\mathcal{F}(\mathbf{x}, \omega_6; \boldsymbol{\alpha}) = f(\mathbf{x}; \boldsymbol{\alpha}) \omega_6$.

To understand the impact of using different possible neural network architectures, we have performed a manual scan over a set of neural network configurations. The input layer has 5 nodes (one per each \mathbf{x} component) and the output layer has one node resulting in a scalar $f(\mathbf{x}; \boldsymbol{\alpha})$. We study networks with a single hidden layer of 1-9 nodes and double hidden layer networks with 1-9 nodes each, constraining the number of nodes on the second hidden layer to be smaller than or at most equal to the number of nodes on the first hidden layer. The results of the converged test losses of 50 different random weight initializations per configuration are shown on Fig. 1 in the purple box plot. The plain ω_6 -based observable is shown in gray, with the dashed lines denoting its 1σ statistical uncertainty. We find that the phase-space optimization of ω_6 gives a noticeable improvement over plain ω_6 when using a large enough network. To test how well the resulting network generalizes to other values of $\tilde{\kappa}$ we use the 50 converged $\{9, 9\}$ models and calculate the dependence of the resulting observable significance with respect to $\tilde{\kappa}$. This is shown on Fig. 2 where a consistent improvement over simple $\langle \omega_6 \rangle$ can be seen at all considered $\tilde{\kappa}$.

As the phase-space optimization of ω_6 gives good results, we now turn to the rest of the ω 's. However, instead of attempting a phase-space optimization of each of them separately, in the next subsection we consider a more general case where the CP -odd observable itself is parameterized with a neural network.

2.2. Neural network as a CP -odd observable

Here we consider a case where the output of the neural network is a CP -odd quantity that defines our observable. We build a network with 14 inputs, one per each ω_i , and

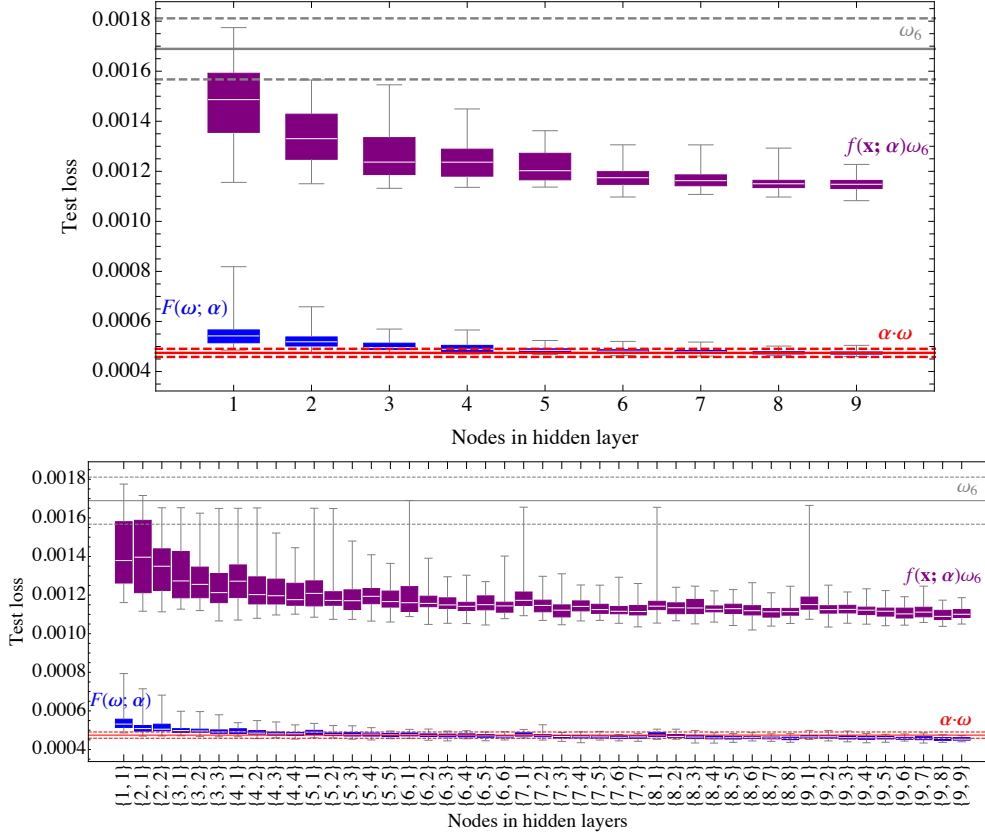


Figure 1: A scan in terms of the test loss (sample size 2.5M) over neural network configurations with one (upper plot) or two (lower plot) hidden layers for the phase-space optimized ω_6 (8) shown in the purple box plot and the generalized $F(\omega)$ (Sec. 2.2) shown in the blue box plot. The spread in both cases corresponds to 50 different random weight initializations per configuration. For comparison the plain ω_6 (2) is shown in gray with the dashed lines showing its 1σ statistical uncertainty. The first order approximation of $F(\omega)$, defined in Eq. (9), is shown in red as described in Sec. 2.3.

one output $F(\omega; \alpha)$, which is correctly anti-symmetrized so that $F(\omega; \alpha) = -F(-\omega; \alpha)$. The loss function is defined in Eq. (4) where now $\mathcal{F}(\mathbf{X}; \alpha) = F(\omega; \alpha)$. Note that since we include the complete irreducible set ω in this non-linear construction, it effectively also covers the case of a simple phase-space optimization of any (linear combination of) ω_i , since all relevant CP-even phase-space variables can be recovered by taking suitable ratios of $\omega_i/\omega_{i'}$.

We again carry out the study of the dependence of the network size with respect to the test sample loss, including non-negligible uncertainties associated with random weight initializations. We scan the neural network architecture parameter space in the same way as in the previous case, starting with a single hidden layer of 1-9 nodes, then adding an additional hidden layer with the number of nodes smaller than or equal to the number of nodes on the first hidden layer. For each configuration we run 50 trainings with different random weight initializations. The results are again shown in Fig. 1, now in the blue

box plot. We find a considerable improvement over the phase-space optimization of the single ω_6 .

Again we check the generalizing power of the resulting observables to other $\tilde{\kappa}$ by fixing the model configuration to $\{9, 9\}$ and calculating the significance of the resulting observables with respect to $\tilde{\kappa}$. The results are shown on Fig. 2. We find a consistent improvement over the previous case across all considered $\tilde{\kappa}$. A noticeable improvement in the significance can be seen. In order to better understand the physics underlying the optimization, we next consider this model in the leading order approximation in ω .

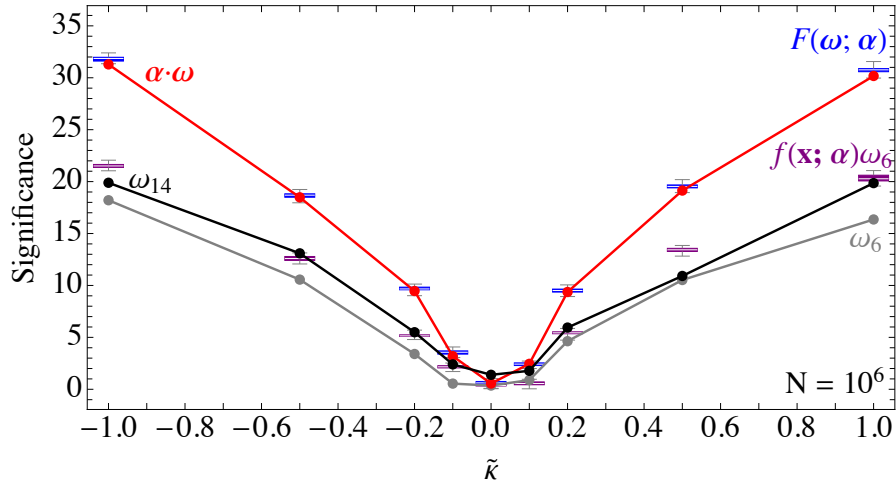


Figure 2: Comparison of the significances of all the observables considered in this work with respect to $\tilde{\kappa}$. The results correspond to 1M events per $\tilde{\kappa}$ at 14 TeV. Plain ω_6 (2) in gray, ω_{14} (3) in black, phase-space optimized ω_6 (8) in purple, anti-symmetrized neural network $F(\omega; \alpha)$ (Sec. 2.2) in blue and the first order approximation of the latter $\alpha \cdot \omega$ in red (Sec. 2.3). See text for details on each observable.

2.3. First order approximation of $F(\omega; \alpha)$

To address the arbitrariness of the neural network architecture choice and to better understand the underlying physics, in this Section we consider the first order ω approximation of the form of $F(\omega; \alpha) = \sum_j \alpha_j \omega_j + \mathcal{O}(\omega^3)$ for $j \in \{1, \dots, 22\}$. The approximation is justifiable in terms of a Taylor expansion, as most of the events have $|\omega_j| \ll 1$.⁵ The observable is then simply

$$\alpha \cdot \omega = \left\langle \sum_j \alpha_j \omega_j \right\rangle, \quad (9)$$

with the subsidiary condition $|\alpha| = 1$. We can optimize over α_j by maximizing the significance

$$\frac{\partial}{\partial \alpha_j} \frac{(\alpha \cdot \omega)_{\text{all}}}{\text{std}((\alpha \cdot \omega)_{\text{all}})} = 0. \quad (10)$$

⁵Note that $|\omega_i| < 1$ by definition, whereas in some cases (also for ω_6) the upper bound is $1/2$. See App. Appendix A.

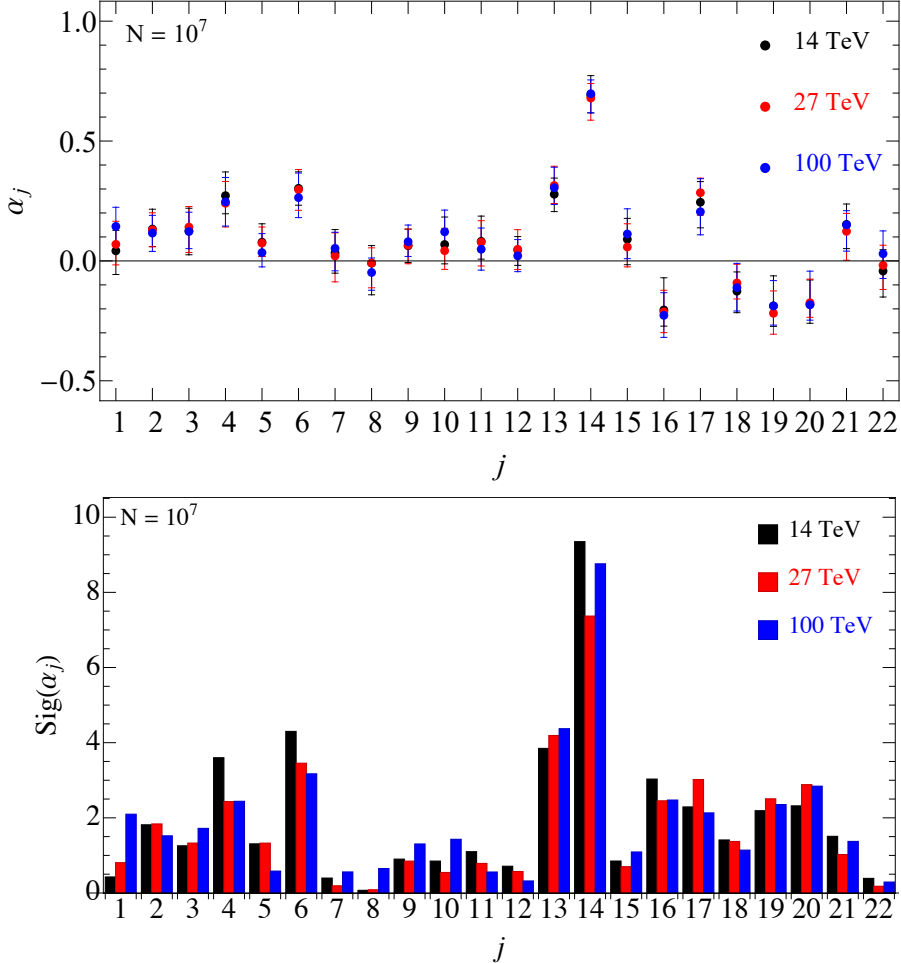


Figure 3: Optimal weights of the linear observable defined in Eq. (9). The upper plot shows uncertainties of α_j , estimated using the expected statistical errors of the observable significances, see text for details. The lower plot shows the significances of α_j (defined as their central value divided by their estimated uncertainty).

Doing so we obtain a system of 22 quadratic equations ⁶

$$\alpha^T M^{(j)} \alpha = 0, \quad (11)$$

where $\alpha = [\alpha_1, \dots, \alpha_{22}]^T$ and 22×22 matrices $M^{(j)}$ are given by

$$M_{ik}^{(j)} = \langle \omega_i \omega_j \rangle \langle \omega_k \rangle - \langle \omega_i \omega_k \rangle \langle \omega_j \rangle. \quad (12)$$

⁶Notice that the problem is equivalent to a single neuron NN with 22 inputs and one output without the activation function or the bias term.

We use this approach to extract the optimal weights α_j from 10^7 events generated with $\tilde{\kappa} = 1$ at 14, 27, and 100 TeV. We estimate the uncertainty associated with the optimal weights in the following way. First we estimate the statistical spread of the significance obtained with optimal α_j . Next we allow α_j to float in the intervals $[\alpha_j - \sigma_j, \alpha_j + \sigma_j]$, where σ_j are chosen such that the decrease of the significance due to the change in α_j corresponds to the statistical spread of the significance. We perform an efficient scan around the optimal vector α in its 22-dimensional neighborhood using spherical coordinates to trivially fulfill the normalization constraint $\sum_j \alpha_j^2 = 1$. We approximate the significance with a quadratic function around the extremum to find independent, uncorrelated directions in the α -space. With this procedure we determine how sharply the optimal α_j are defined. We estimate the statistical error of the significance using 10^7 events. Clearly the uncertainties σ_j are larger for smaller chosen sample size. The results of this approach are shown in Fig. 3, where the upper (lower) panel shows the estimated error (significance) for each α_j at 14, 27, and 100 TeV. A comparison of the observable $\alpha \cdot \omega$ to other approaches in this work is shown in Fig. 2. We reach a similar level of improvement compared to the full $F(\omega; \alpha)$ network with significantly fewer parameters.

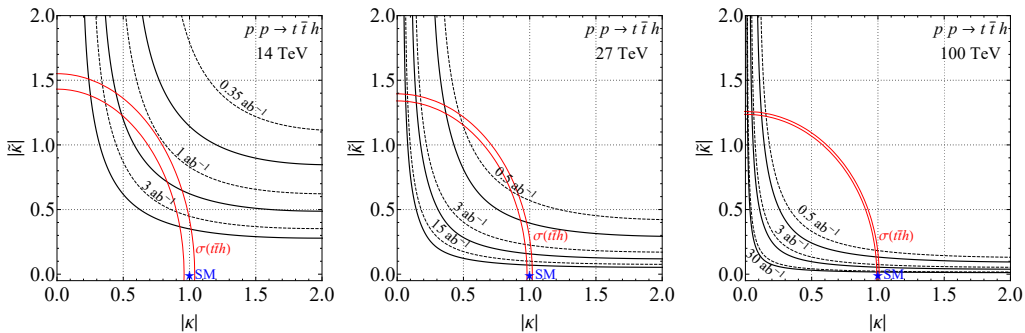


Figure 4: The 2σ exclusion zones in the $\kappa - \tilde{\kappa}$ plane by assuming a null result at HL-LHC, HE-LHC and FCC-hh for different luminosities. The optimized observable $\alpha \cdot \omega$ is shown in solid black, while the plain ω_6 (2) results are shown using dashed lines. The projected sensitivity of $t\bar{t}h$ production cross-section measurements is shown in red, see text for details. At 14 TeV order 1 exclusion of $\tilde{\kappa}$ can be achieved using $\alpha \cdot \omega$ with 350 fb^{-1} which corresponds to the final integrated luminosity of the LHC.

3. Bounds in the $(\kappa, \tilde{\kappa})$ plane

We produce the bounds in the $(\kappa, \tilde{\kappa})$ plane by including showering and hadronization effects using **Pythia8** and detector effects using **Delphes** with the default ATLAS simulation card. As the $t\bar{t}h$ is followed by semileptonic top decays and $h \rightarrow b\bar{b}$ decay, our signal is defined as 4 b -jets and two oppositely charged leptons ℓ . We include the main irreducible background $pp \rightarrow t\bar{t}b\bar{b}$ with both tops decaying semileptonically and use the same event selection requirements as in Section 3.2 of [24], where the results of using plain ω_6 are shown. We update those bounds for HL- and HE-LHC and produce bounds for FCC-hh for the first time by using the optimal observable (9) with the weights shown in the upper plot of Fig. 3. The results of assuming a null result up to the expected statistical uncertainty for different luminosities at different energies are shown on Fig. 4,

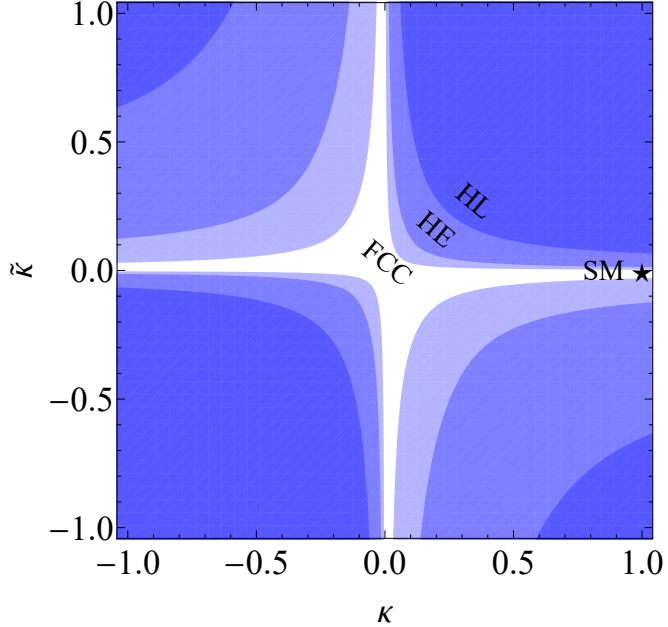


Figure 5: The 2σ exclusion regions at HL-LHC (3 ab^{-1}), HE-LHC (15 ab^{-1}) and FCC-hh (30 ab^{-1}) by assuming a measurement of a 2σ positive fluctuation in the optimal observable $\alpha \cdot \omega$ (9).

where we also show the expected sensitivity to $(\kappa, \tilde{\kappa})$ from the $t\bar{t}h$ production cross-section measurements using the projected uncertainties of $\delta\kappa/\kappa \sim (0.04, 0.02, 0.009)$ at HL-LHC, HE-LHC [41] and FCC-hh [42], respectively.

A consistent improvement of sensitivity can be achieved by using the optimized combination of ω 's with respect to a single ω_6 , constraining the parameter space significantly in orthogonal directions compared to the cross-section measurements. Interestingly the significance improvement is consistent between partonic events and after including shower, detector effects, as well as the dominant background and realistic object reconstruction, even though the optimization was performed at parton level only. This robustness is a welcome benefit of the method, since the computationally costly optimization procedure does not appear to be sensitive to modeling of the hadronic final states and detector effects. It is also reassuring that the optimization does not significantly rely on specific phase-space regions particularly affected by the background. We expect the results to be also robust against higher order QCD corrections. In Ref. [24] we have explicitly compared how the inclusion of NLO QCD effects changes the optimized observables in the case of $pp \rightarrow thj$ and found a shift of the optimal weight function smaller than 10%.

We show the sensitivity of the optimized observable to the sign of $\tilde{\kappa}$ (and κ) on Fig. 5 by assuming the measurement of a 2σ positive statistical fluctuation of the SM case, which in our estimate corresponds to the measurement of $\alpha \cdot \omega = (4.6 \pm 2.3) \times 10^{-4}$, $\alpha \cdot \omega = (0.9 \pm 0.45) \times 10^{-4}$ and $\alpha \cdot \omega = (0.2 \pm 0.1) \times 10^{-4}$ for HL-LHC (3 ab^{-1}), HE-LHC (15 ab^{-1}) and FCC-hh (30 ab^{-1}) respectively.

4. Summary and conclusions

Introducing a set of manifestly CP -odd observables (ω_i) built from experimentally accessible final state momenta in $pp \rightarrow t\bar{t}h$ production with semileptonically decaying tops, we studied the prospect of their phase-space optimization, parameterizing the optimal weight functions with neural networks. First we considered the phase-space optimization of a single ω_6 , improving its performance. Next we studied a general CP -odd observable, parameterized directly by an anti-symmetric neural network, which ended with an even higher performance boost. Lastly we studied the first order approximation of this network as a linear combination of the CP -odd observables, producing a simpler and more robust observable. The benefit of using the optimized observable, although marginal for realistic numbers of events, especially at the HL-LHC, carries over from parton level final states to the analysis at event reconstruction level, resulting in projections of probing $\tilde{\kappa}$ directly at HL-LHC, HE-LHC and FCC-hh. We found that the LHC at the end of Run 3 will exclude $\kappa\tilde{\kappa} \sim 1$ with 2σ confidence, while FCC-hh would ultimately be sensitive to $\kappa\tilde{\kappa} \sim 0.01$. Finally, our approach to parametrizing CP -odd observables over high-dimensional phase-spaces using manifestly CP -odd NNs could be applied to other high energy particle production and decay processes, as well as to other symmetries. We leave the exploration of these ideas for future work.

Acknowledgments

The authors acknowledge the financial support from the Slovenian Research Agency (research core funding No. P1-0035 and J1-8137). This article is based upon work from COST Action CA16201 PARTICLEFACE supported by COST (European Cooperation in Science and Technology). A. S. is supported by the Young Researchers Programme of the Slovenian Research Agency under the grant No. 50510, core funding grant P1-0035.

Appendix A. Construction of $\omega_1, \dots, \omega_{22}$

In this Section we derive the most general set of linearly independent pseudoscalars of mass-dimension 5 that are even under charge conjugation and under $b \leftrightarrow \bar{b}$. It is convenient to start from 5 independent 3-vectors with well-defined C : $V \in \{\mathbf{p}_h, \mathbf{p}_{\ell-} + \mathbf{p}_{\ell+}, \mathbf{p}_{\ell-} - \mathbf{p}_{\ell+}, \mathbf{p}_b + \mathbf{p}_{\bar{b}}, \mathbf{p}_b - \mathbf{p}_{\bar{b}}\}$. All of the quintuple products with desired properties can be expressed as $\omega \sim V_1 \times V_2 \cdot V_3 V_4 \cdot V_5$.⁷ We can find systematically all ω 's by considering 10 distinct mixed products $V_1 \times V_2 \cdot V_3$. Multiplying these together with 15 different $V_4 \cdot V_5$ we have 150 potential quintuple products. In the last step we symmetrize the obtained product with respect to C -conjugation and $b \leftrightarrow \bar{b}$ and we find that only a handful of ω 's remain, which we list below.

In order to reduce the number of linearly independent ω 's we have employed an Euclidean tensor identity

$$\delta_{ab}\epsilon_{cde} - \delta_{ac}\epsilon_{deb} + \delta_{ad}\epsilon_{ebc} - \delta_{ae}\epsilon_{bcd} = 0, \quad (\text{A.1})$$

⁷Notice that the possibility of a nested cross product $((V_1 \times V_2) \times V_3) \times V_4 \cdot V_5$ can also be reduced to this form.

or, equivalently, that the following linear combination of four arbitrary vectors vanishes:

$$\mathbf{a}(\mathbf{b} \times \mathbf{c} \cdot \mathbf{d}) - \mathbf{b}(\mathbf{c} \times \mathbf{d} \cdot \mathbf{a}) + \mathbf{c}(\mathbf{d} \times \mathbf{a} \cdot \mathbf{b}) - \mathbf{d}(\mathbf{a} \times \mathbf{b} \cdot \mathbf{c}) = 0, \quad (\text{A.2})$$

to eliminate some of the quintuple products. The sign before individual terms in the last expression corresponds to the sign of the cyclic permutation of the four vectors.

The first class of ω 's involves \mathbf{p}_{ℓ^+} and \mathbf{p}_{ℓ^-} in the mixed product, $\mathbf{p}_{\ell^-} - \mathbf{p}_{\ell^+}$ in the scalar product. Both products are even under $b \leftrightarrow \bar{b}$:

$$\omega_1 \sim [(\mathbf{p}_{\ell^-} \times \mathbf{p}_{\ell^+}) \cdot \mathbf{p}_h] [(\mathbf{p}_{\ell^-} - \mathbf{p}_{\ell^+}) \cdot \mathbf{p}_h], \quad (\text{A.3})$$

$$\omega_2 \sim [(\mathbf{p}_{\ell^-} \times \mathbf{p}_{\ell^+}) \cdot \mathbf{p}_h] [(\mathbf{p}_{\ell^-} - \mathbf{p}_{\ell^+}) \cdot (\mathbf{p}_{\ell^+} + \mathbf{p}_{\ell^+})], \quad (\text{A.4})$$

$$\omega_3 \sim [(\mathbf{p}_{\ell^-} \times \mathbf{p}_{\ell^+}) \cdot \mathbf{p}_h] [(\mathbf{p}_{\ell^-} - \mathbf{p}_{\ell^+}) \cdot (\mathbf{p}_b + \mathbf{p}_{\bar{b}})], \quad (\text{A.5})$$

$$\omega_4 \sim [(\mathbf{p}_{\ell^-} \times \mathbf{p}_{\ell^+}) \cdot (\mathbf{p}_b + \mathbf{p}_{\bar{b}})] [(\mathbf{p}_{\ell^-} - \mathbf{p}_{\ell^+}) \cdot \mathbf{p}_h], \quad (\text{A.6})$$

$$\omega_5 \sim [(\mathbf{p}_{\ell^-} \times \mathbf{p}_{\ell^+}) \cdot (\mathbf{p}_b + \mathbf{p}_{\bar{b}})] [(\mathbf{p}_{\ell^-} - \mathbf{p}_{\ell^+}) \cdot (\mathbf{p}_{\ell^-} + \mathbf{p}_{\ell^+})], \quad (\text{A.7})$$

$$\omega_6 \sim [(\mathbf{p}_{\ell^-} \times \mathbf{p}_{\ell^+}) \cdot (\mathbf{p}_b + \mathbf{p}_{\bar{b}})] [(\mathbf{p}_{\ell^-} - \mathbf{p}_{\ell^+}) \cdot (\mathbf{p}_b + \mathbf{p}_{\bar{b}})]. \quad (\text{A.8})$$

The second class involves $\mathbf{p}_b \times \mathbf{p}_{\bar{b}}$ and/or $\mathbf{p}_b - \mathbf{p}_{\bar{b}}$ in both mixed and scalar products:

$$\omega_7 \sim [(\mathbf{p}_b \times \mathbf{p}_{\bar{b}}) \cdot \mathbf{p}_h] [(\mathbf{p}_b - \mathbf{p}_{\bar{b}}) \cdot \mathbf{p}_h], \quad (\text{A.9})$$

$$\omega_8 \sim [(\mathbf{p}_b \times \mathbf{p}_{\bar{b}}) \cdot \mathbf{p}_h] [(\mathbf{p}_b - \mathbf{p}_{\bar{b}}) \cdot (\mathbf{p}_{\ell^-} + \mathbf{p}_{\ell^+})], \quad (\text{A.10})$$

$$\omega_9 \sim [(\mathbf{p}_b \times \mathbf{p}_{\bar{b}}) \cdot \mathbf{p}_h] [(\mathbf{p}_b - \mathbf{p}_{\bar{b}}) \cdot (\mathbf{p}_b + \mathbf{p}_{\bar{b}})], \quad (\text{A.11})$$

$$\omega_{10} \sim [(\mathbf{p}_b \times \mathbf{p}_{\bar{b}}) \cdot (\mathbf{p}_{\ell^-} + \mathbf{p}_{\ell^+})] [(\mathbf{p}_b - \mathbf{p}_{\bar{b}}) \cdot \mathbf{p}_h], \quad (\text{A.12})$$

$$\omega_{11} \sim [(\mathbf{p}_b \times \mathbf{p}_{\bar{b}}) \cdot (\mathbf{p}_{\ell^-} + \mathbf{p}_{\ell^+})] [(\mathbf{p}_b - \mathbf{p}_{\bar{b}}) \cdot (\mathbf{p}_{\ell^-} + \mathbf{p}_{\ell^+})], \quad (\text{A.13})$$

$$\omega_{12} \sim [(\mathbf{p}_b \times \mathbf{p}_{\bar{b}}) \cdot (\mathbf{p}_{\ell^-} + \mathbf{p}_{\ell^+})] [(\mathbf{p}_b - \mathbf{p}_{\bar{b}}) \cdot (\mathbf{p}_b + \mathbf{p}_{\bar{b}})], \quad (\text{A.14})$$

$$\omega_{13} \sim [(\mathbf{p}_b \times \mathbf{p}_{\bar{b}}) \cdot (\mathbf{p}_{\ell^-} - \mathbf{p}_{\ell^+})] [(\mathbf{p}_b - \mathbf{p}_{\bar{b}}) \cdot (\mathbf{p}_{\ell^-} - \mathbf{p}_{\ell^+})], \quad (\text{A.15})$$

$$\omega_{14} \sim [(\mathbf{p}_{\ell^-} \times \mathbf{p}_{\ell^+}) \cdot (\mathbf{p}_b - \mathbf{p}_{\bar{b}})] [(\mathbf{p}_b - \mathbf{p}_{\bar{b}}) \cdot (\mathbf{p}_{\ell^-} - \mathbf{p}_{\ell^+})]. \quad (\text{A.16})$$

The third class involves mixed product of \mathbf{p}_h , $\mathbf{p}_{\ell^-} \pm \mathbf{p}_{\ell^+}$, and $\mathbf{p}_b \pm \mathbf{p}_{\bar{b}}$:

$$\omega_{15} \sim [\mathbf{p}_h \times (\mathbf{p}_{\ell^-} + \mathbf{p}_{\ell^+}) \cdot (\mathbf{p}_b - \mathbf{p}_{\bar{b}})] [(\mathbf{p}_b - \mathbf{p}_{\bar{b}}) \cdot \mathbf{p}_h], \quad (\text{A.17})$$

$$\omega_{16} \sim [\mathbf{p}_h \times (\mathbf{p}_{\ell^-} + \mathbf{p}_{\ell^+}) \cdot (\mathbf{p}_b - \mathbf{p}_{\bar{b}})] [(\mathbf{p}_b - \mathbf{p}_{\bar{b}}) \cdot (\mathbf{p}_{\ell^-} + \mathbf{p}_{\ell^+})], \quad (\text{A.18})$$

$$\omega_{17} \sim [\mathbf{p}_h \times (\mathbf{p}_{\ell^-} + \mathbf{p}_{\ell^+}) \cdot (\mathbf{p}_b - \mathbf{p}_{\bar{b}})] [(\mathbf{p}_b - \mathbf{p}_{\bar{b}}) \cdot (\mathbf{p}_b + \mathbf{p}_{\bar{b}})], \quad (\text{A.19})$$

$$\omega_{18} \sim [\mathbf{p}_h \times (\mathbf{p}_{\ell^-} - \mathbf{p}_{\ell^+}) \cdot (\mathbf{p}_b + \mathbf{p}_{\bar{b}})] [(\mathbf{p}_{\ell^-} - \mathbf{p}_{\ell^+}) \cdot \mathbf{p}_h], \quad (\text{A.20})$$

$$\omega_{19} \sim [\mathbf{p}_h \times (\mathbf{p}_{\ell^-} - \mathbf{p}_{\ell^+}) \cdot (\mathbf{p}_b + \mathbf{p}_{\bar{b}})] [(\mathbf{p}_{\ell^-} - \mathbf{p}_{\ell^+}) \cdot (\mathbf{p}_{\ell^-} + \mathbf{p}_{\ell^+})], \quad (\text{A.21})$$

$$\omega_{20} \sim [\mathbf{p}_h \times (\mathbf{p}_{\ell^-} - \mathbf{p}_{\ell^+}) \cdot (\mathbf{p}_b + \mathbf{p}_{\bar{b}})] [(\mathbf{p}_{\ell^-} - \mathbf{p}_{\ell^+}) \cdot (\mathbf{p}_b + \mathbf{p}_{\bar{b}})], \quad (\text{A.22})$$

$$\omega_{21} \sim [\mathbf{p}_h \times (\mathbf{p}_{\ell^-} - \mathbf{p}_{\ell^+}) \cdot (\mathbf{p}_b - \mathbf{p}_{\bar{b}})] [(\mathbf{p}_{\ell^-} - \mathbf{p}_{\ell^+}) \cdot (\mathbf{p}_b - \mathbf{p}_{\bar{b}})]. \quad (\text{A.23})$$

There are further possibilities with a mixed product $\mathbf{p}_h \times (\mathbf{p}_{\ell^-} + \mathbf{p}_{\ell^+}) \cdot (\mathbf{p}_b + \mathbf{p}_{\bar{b}})$ multiplied by one of 8 C-even, $b \leftrightarrow \bar{b}$ even scalar products $\{\mathbf{p}_h \cdot \mathbf{p}_h, \mathbf{p}_h \cdot (\mathbf{p}_{\ell^-} + \mathbf{p}_{\ell^+}), \mathbf{p}_h \cdot (\mathbf{p}_b + \mathbf{p}_{\bar{b}}), (\mathbf{p}_{\ell^-} + \mathbf{p}_{\ell^+}) \cdot (\mathbf{p}_b + \mathbf{p}_{\bar{b}}), (\mathbf{p}_{\ell^-} \pm \mathbf{p}_{\ell^+})^2, (\mathbf{p}_b \pm \mathbf{p}_{\bar{b}})^2\}$. Since the mixed product itself already has the desired symmetry properties, those 8 quintuple products do not bring additional new information, with respect to a mixed (triple) product that is our final observable:

$$\omega_{22} \sim \mathbf{p}_h \times (\mathbf{p}_{\ell^-} + \mathbf{p}_{\ell^+}) \cdot (\mathbf{p}_b + \mathbf{p}_{\bar{b}}). \quad (\text{A.24})$$

Note that there are nonlinear relations between ω 's, such as $\omega_1\omega_6 = \omega_3\omega_4$, that we do not exploit to further reduce the set. Namely, ratios of ω 's can contain singularities in the available phase-space and as such would be difficult to reconstruct by a neural network optimizer.

All the ω 's are normalized by the lengths of the vectors that enter as factors in the scalar products,

$$\omega_i = \frac{[\mathbf{V}_1 \times \mathbf{V}_2 \cdot \mathbf{V}_3][\mathbf{V}_4 \cdot \mathbf{V}_5]}{|\mathbf{V}_1 \times \mathbf{V}_2| |\mathbf{V}_3| |\mathbf{V}_4| |\mathbf{V}_5|}, \quad (\text{A.25})$$

and the upper bound $|\omega_i| \leq 1$ is generally valid. For cases when ω_i has a vector \mathbf{a} present both in the mixed and scalar products, e.g. $(\mathbf{V}_1 \times \mathbf{V}_2 \cdot \mathbf{a})(\mathbf{V}_3 \cdot \mathbf{a})$, and furthermore with $\mathbf{V}_1 \times \mathbf{V}_2 \cdot \mathbf{V}_3 = 0$, a stricter upper bound $|\omega_i| \leq 1/2$ applies (for $\omega_{1,6,7,11,13,14,15,16,20,21}$).

References

- [1] J. A. Aguilar-Saavedra, A Minimal set of top-Higgs anomalous couplings, *Nucl. Phys. B* 821 (2009) 215–227. [arXiv:0904.2387](https://arxiv.org/abs/0904.2387), [doi:10.1016/j.nuclphysb.2009.06.022](https://doi.org/10.1016/j.nuclphysb.2009.06.022).
- [2] J. Ellis, D. S. Hwang, K. Sakurai, M. Takeuchi, Disentangling Higgs-Top Couplings in Associated Production, *JHEP* 04 (2014) 004. [arXiv:1312.5736](https://arxiv.org/abs/1312.5736), [doi:10.1007/JHEP04\(2014\)004](https://doi.org/10.1007/JHEP04(2014)004).
- [3] G. Aad, et al., Measurements of the Higgs boson production and decay rates and constraints on its couplings from a combined ATLAS and CMS analysis of the LHC pp collision data at $\sqrt{s} = 7$ and 8 TeV, *JHEP* 08 (2016) 045. [arXiv:1606.02266](https://arxiv.org/abs/1606.02266), [doi:10.1007/JHEP08\(2016\)045](https://doi.org/10.1007/JHEP08(2016)045).
- [4] G. Bhattacharyya, D. Das, P. B. Pal, Modified Higgs couplings and unitarity violation, *Phys. Rev. D* 87 (2013) 011702. [arXiv:1212.4651](https://arxiv.org/abs/1212.4651), [doi:10.1103/PhysRevD.87.011702](https://doi.org/10.1103/PhysRevD.87.011702).
- [5] B. Grzadkowski, J. F. Gunion, Using decay angle correlations to detect CP violation in the neutral Higgs sector, *Phys. Lett. B* 350 (1995) 218–224. [arXiv:hep-ph/9501339](https://arxiv.org/abs/hep-ph/9501339), [doi:10.1016/0370-2693\(95\)00369-V](https://doi.org/10.1016/0370-2693(95)00369-V).
- [6] F. Demartin, F. Maltoni, K. Mawatari, B. Page, M. Zaro, Higgs characterisation at NLO in QCD: CP properties of the top-quark Yukawa interaction, *Eur. Phys. J. C* 74 (9) (2014) 3065. [arXiv:1407.5089](https://arxiv.org/abs/1407.5089), [doi:10.1140/epjc/s10052-014-3065-2](https://doi.org/10.1140/epjc/s10052-014-3065-2).
- [7] F. Boudjema, R. M. Godbole, D. Guadagnoli, K. A. Mohan, Lab-frame observables for probing the top-Higgs interaction, *Phys. Rev. D* 92 (1) (2015) 015019. [arXiv:1501.03157](https://arxiv.org/abs/1501.03157), [doi:10.1103/PhysRevD.92.015019](https://doi.org/10.1103/PhysRevD.92.015019).
- [8] M. R. Buckley, D. Goncalves, Boosting the Direct CP Measurement of the Higgs-Top Coupling, *Phys. Rev. Lett.* 116 (9) (2016) 091801. [arXiv:1507.07926](https://arxiv.org/abs/1507.07926), [doi:10.1103/PhysRevLett.116.091801](https://doi.org/10.1103/PhysRevLett.116.091801).
- [9] N. Mileo, K. Kiers, A. Szynkman, D. Crane, E. Gegner, Pseudoscalar top-Higgs coupling: exploration of CP-odd observables to resolve the sign ambiguity, *JHEP* 07 (2016) 056. [arXiv:1603.03632](https://arxiv.org/abs/1603.03632), [doi:10.1007/JHEP07\(2016\)056](https://doi.org/10.1007/JHEP07(2016)056).
- [10] A. V. Gritsan, R. Röntsch, M. Schulze, M. Xiao, Constraining anomalous Higgs boson couplings to the heavy flavor fermions using matrix element techniques, *Phys. Rev. D* 94 (5) (2016) 055023. [arXiv:1606.03107](https://arxiv.org/abs/1606.03107), [doi:10.1103/PhysRevD.94.055023](https://doi.org/10.1103/PhysRevD.94.055023).
- [11] J. Li, Z.-g. Si, L. Wu, J. Yue, Central-edge asymmetry as a probe of Higgs-top coupling in $t\bar{t}h$ production at the LHC, *Phys. Lett. B* 779 (2018) 72–76. [arXiv:1701.00224](https://arxiv.org/abs/1701.00224), [doi:10.1016/j.physletb.2018.02.009](https://doi.org/10.1016/j.physletb.2018.02.009).
- [12] S. Amor Dos Santos, et al., Probing the CP nature of the Higgs coupling in $t\bar{t}h$ events at the LHC, *Phys. Rev. D* 96 (1) (2017) 013004. [arXiv:1704.03565](https://arxiv.org/abs/1704.03565), [doi:10.1103/PhysRevD.96.013004](https://doi.org/10.1103/PhysRevD.96.013004).
- [13] D. Gonçalves, K. Kong, J. H. Kim, Probing the top-Higgs Yukawa CP structure in dileptonic $t\bar{t}h$ with M_2 -assisted reconstruction, *JHEP* 06 (2018) 079. [arXiv:1804.05874](https://arxiv.org/abs/1804.05874), [doi:10.1007/JHEP06\(2018\)079](https://doi.org/10.1007/JHEP06(2018)079).
- [14] A. Kobakhidze, L. Wu, J. Yue, Anomalous Top-Higgs Couplings and Top Polarisation in Single Top and Higgs Associated Production at the LHC, *JHEP* 10 (2014) 100. [arXiv:1406.1961](https://arxiv.org/abs/1406.1961), [doi:10.1007/JHEP10\(2014\)100](https://doi.org/10.1007/JHEP10(2014)100).
- [15] J. Yue, Enhanced thj signal at the LHC with $h \rightarrow \gamma\gamma$ decay and \mathcal{CP} -violating top-Higgs coupling, *Phys. Lett. B* 744 (2015) 131–136. [arXiv:1410.2701](https://arxiv.org/abs/1410.2701), [doi:10.1016/j.physletb.2015.03.044](https://doi.org/10.1016/j.physletb.2015.03.044).

[16] F. Demartin, F. Maltoni, K. Mawatari, M. Zaro, Higgs production in association with a single top quark at the LHC, *Eur. Phys. J. C* 75 (6) (2015) 267. [arXiv:1504.00611](https://arxiv.org/abs/1504.00611), [doi:10.1140/epjc/s10052-015-3475-9](https://doi.org/10.1140/epjc/s10052-015-3475-9).

[17] V. Barger, K. Hagiwara, Y.-J. Zheng, Probing the Higgs Yukawa coupling to the top quark at the LHC via single top+Higgs production, *Phys. Rev. D* 99 (3) (2019) 031701. [arXiv:1807.00281](https://arxiv.org/abs/1807.00281), [doi:10.1103/PhysRevD.99.031701](https://doi.org/10.1103/PhysRevD.99.031701).

[18] M. Kraus, T. Martini, S. Peitzsch, P. Uwer, Exploring BSM Higgs couplings in single top-quark production [arXiv:1908.09100](https://arxiv.org/abs/1908.09100).

[19] W. Bernreuther, A. Brandenburg, Tracing CP violation in the production of top quark pairs by multiple TeV proton proton collisions, *Phys. Rev. D* 49 (1994) 4481–4492. [arXiv:hep-ph/9312210](https://arxiv.org/abs/hep-ph/9312210), [doi:10.1103/PhysRevD.49.4481](https://doi.org/10.1103/PhysRevD.49.4481).

[20] V. Barger, K. Hagiwara, Y.-J. Zheng, Probing the top Yukawa coupling at the LHC via associated production of single top and Higgs [arXiv:1912.11795](https://arxiv.org/abs/1912.11795).

[21] R. Patrick, A. Scaffidi, P. Sharma, Top polarisation as a probe of CP-mixing top-Higgs coupling in tjh signals, *Phys. Rev. D* 101 (9) (2020) 093005. [arXiv:1909.12772](https://arxiv.org/abs/1909.12772), [doi:10.1103/PhysRevD.101.093005](https://doi.org/10.1103/PhysRevD.101.093005).

[22] A. Ferroglio, M. C. Fiolhais, E. Gouveia, A. Onofre, Role of the $t\bar{t}h$ rest frame in direct top-quark Yukawa coupling measurements, *Phys. Rev. D* 100 (7) (2019) 075034. [arXiv:1909.00490](https://arxiv.org/abs/1909.00490), [doi:10.1103/PhysRevD.100.075034](https://doi.org/10.1103/PhysRevD.100.075034).

[23] J. Brod, U. Haisch, J. Zupan, Constraints on CP-violating Higgs couplings to the third generation, *JHEP* 11 (2013) 180. [arXiv:1310.1385](https://arxiv.org/abs/1310.1385), [doi:10.1007/JHEP11\(2013\)180](https://doi.org/10.1007/JHEP11(2013)180).

[24] D. A. Faroughy, J. F. Kamenik, N. Košnik, A. Smolkovič, Probing the CP nature of the top quark Yukawa at hadron colliders, *JHEP* 02 (2020) 085. [arXiv:1909.00007](https://arxiv.org/abs/1909.00007), [doi:10.1007/JHEP02\(2020\)085](https://doi.org/10.1007/JHEP02(2020)085).

[25] G. Durieux, Y. Grossman, Probing CP violation systematically in differential distributions, *Phys. Rev. D* 92 (7) (2015) 076013. [arXiv:1508.03054](https://arxiv.org/abs/1508.03054), [doi:10.1103/PhysRevD.92.076013](https://doi.org/10.1103/PhysRevD.92.076013).

[26] W. Bernreuther, A. Brandenburg, Tracing CP violation in the production of top quark pairs by multiple TeV proton proton collisions, *Phys. Rev. D* 49 (1994) 4481–4492. [arXiv:hep-ph/9312210](https://arxiv.org/abs/hep-ph/9312210), [doi:10.1103/PhysRevD.49.4481](https://doi.org/10.1103/PhysRevD.49.4481).

[27] J. Brehmer, F. Kling, I. Espejo, K. Cranmer, MadMiner: Machine learning-based inference for particle physics, *Comput. Softw. Big Sci.* 4 (1) (2020) 3. [arXiv:1907.10621](https://arxiv.org/abs/1907.10621), [doi:10.1007/s41781-020-0035-2](https://doi.org/10.1007/s41781-020-0035-2).

[28] High-Luminosity Large Hadron Collider (HL-LHC): Technical Design Report V. 0.1 4/2017. [doi:10.23731/CYRM-2017-004](https://doi.org/10.23731/CYRM-2017-004).

[29] Projected Performance of an Upgraded CMS Detector at the LHC and HL-LHC: Contribution to the Snowmass Process, in: Community Summer Study 2013: Snowmass on the Mississippi, 2013. [arXiv:1307.7135](https://arxiv.org/abs/1307.7135).

[30] Physics at a High-Luminosity LHC with ATLAS, in: Community Summer Study 2013: Snowmass on the Mississippi, 2013. [arXiv:1307.7292](https://arxiv.org/abs/1307.7292).

[31] F. Zimmermann, et al., High-Energy LHC Design, *J. Phys. Conf. Ser.* 1067 (2) (2018) 022009. [doi:10.1088/1742-6596/1067/2/022009](https://doi.org/10.1088/1742-6596/1067/2/022009).

[32] A. Abada, et al., HE-LHC: The High-Energy Large Hadron Collider: Future Circular Collider Conceptual Design Report Volume 4, *Eur. Phys. J. ST* 228 (5) (2019) 1109–1382. [doi:10.1140/epjst/e2019-900088-6](https://doi.org/10.1140/epjst/e2019-900088-6).

[33] M. L. Mangano, et al., Physics at a 100 TeV pp Collider: Standard Model Processes, *CERN Yellow Rep.* (3) (2017) 1–254. [arXiv:1607.01831](https://arxiv.org/abs/1607.01831), [doi:10.23731/CYRM-2017-003.1](https://doi.org/10.23731/CYRM-2017-003.1).

[34] R. Contino, et al., Physics at a 100 TeV pp collider: Higgs and EW symmetry breaking studies, *CERN Yellow Rep.* (3) (2017) 255–440. [arXiv:1606.09408](https://arxiv.org/abs/1606.09408), [doi:10.23731/CYRM-2017-003.255](https://doi.org/10.23731/CYRM-2017-003.255).

[35] A. Abada, et al., FCC-hh: The Hadron Collider, *Eur. Phys. J. ST* 228 (4) (2019) 755–1107. [doi:10.1140/epjst/e2019-900087-0](https://doi.org/10.1140/epjst/e2019-900087-0).

[36] M. Abadi, A. Agarwal, P. Barham, E. Brevdo, Z. Chen, C. Citro, G. S. Corrado, A. Davis, J. Dean, M. Devin, S. Ghemawat, I. Goodfellow, A. Harp, G. Irving, M. Isard, Y. Jia, R. Jozefowicz, L. Kaiser, M. Kudlur, J. Levenberg, D. Mané, R. Monga, S. Moore, D. Murray, C. Olah, M. Schuster, J. Shlens, B. Steiner, I. Sutskever, K. Talwar, P. Tucker, V. Vanhoucke, V. Vasudevan, F. Viégas, O. Vinyals, P. Warden, M. Wattenberg, M. Wicke, Y. Yu, X. Zheng, *TensorFlow: Large-scale machine learning on heterogeneous systems*, software available from tensorflow.org (2015). URL <http://tensorflow.org/>

[37] J. Alwall, R. Frederix, S. Frixione, V. Hirschi, F. Maltoni, O. Mattelaer, H. S. Shao, T. Stelzer, P. Torrielli, M. Zaro, The automated computation of tree-level and next-to-leading order differential

cross sections, and their matching to parton shower simulations, JHEP 07 (2014) 079. [arXiv:1405.0301](https://arxiv.org/abs/1405.0301), [doi:10.1007/JHEP07\(2014\)079](https://doi.org/10.1007/JHEP07(2014)079).

- [38] J. Bergstra, D. Yamins, D. D. Cox, Making a science of model search: Hyperparameter optimization in hundreds of dimensions for vision architectures, in: Proceedings of the 30th International Conference on International Conference on Machine Learning - Volume 28, ICML'13, JMLR.org, 2013, p. I-115–I-123.
- [39] J. M. Clavijo, P. Glaysher, J. M. Katzy, Adversarial domain adaptation to reduce sample bias of a high energy physics classifier [arXiv:2005.00568](https://arxiv.org/abs/2005.00568).
- [40] D. Atwood, A. Soni, Analysis for magnetic moment and electric dipole moment form-factors of the top quark via $e^+e^- \rightarrow t\bar{t}$, Phys. Rev. D45 (1992) 2405–2413. [doi:10.1103/PhysRevD.45.2405](https://doi.org/10.1103/PhysRevD.45.2405).
- [41] M. Cepeda, et al., Report from Working Group 2: Higgs Physics at the HL-LHC and HE-LHC, Vol. 7, 2019, pp. 221–584. [arXiv:1902.00134](https://arxiv.org/abs/1902.00134), [doi:10.23731/CYRM-2019-007.221](https://doi.org/10.23731/CYRM-2019-007.221).
- [42] A. Abada, et al., FCC Physics Opportunities: Future Circular Collider Conceptual Design Report Volume 1, Eur. Phys. J. C 79 (6) (2019) 474. [doi:10.1140/epjc/s10052-019-6904-3](https://doi.org/10.1140/epjc/s10052-019-6904-3).